Microporous and Mesoporous Materials 274 (2019) 236–244

Contents lists available at ScienceDirect

Microporous and Mesoporous Materials

journal homepage: www.elsevier.com/locate/micromeso

Hierarchical nanoporous activated carbon as potential electrode materials for high performance electrochemical supercapacitor

T. Kesavan, T. Partheeban, M. Vivekanantha, M. Kundu, G. Maduraiveeran*, M. Sasidharan**

Research Institute & Department of Chemistry, SRM Institute of Science and Technology, Kattankulathur, Chennai, 603 203, Tamil Nadu, India

ARTICLE INFO

Keywords:
Nanoporous activated carbon
High specific capacitance
Supercapacitors
Template-free synthesis
Indian cake rusk

ABSTRACT

Recently, biomass-derived activated carbon nanomaterials represent a potential candidate in achieving sustainable and low-cost energy storage devices. Herein, we report a facile synthesis of hierarchical nanoporous activated carbon (NAC) by template-free and cost effective approach using bio-derived food waste namely "Indian Cake Rusk" (ICR) and its application in high performance supercapacitors for the first time. The influence of carbon activation process over the physicochemical properties, morphological structure, as well as supercapacitive performance was systematically studied. When used as an electrode in a supercapacitor, the as-synthesized NAC material offered a high specific capacitance of 381.0 F g^{-1} at a current density of 1.7 A g^{-1} with an impressive 95% capacity retention even after 6000 cycles using 1.0 M H_2SO_4 electrolyte. The NAC material also furnished a maximum energy density of 47.1 Wh kg^{-1} and power density of 22644.0 W kg^{-1} which is higher than the existing carbon based electrode using 1.0 M $LiPF_6$ electrolyte in symmetric supercapacitor. The superior electrochemical performance of NAC material is ascribed to huge BET surface area (1413.0 $m^2 g^{-1}$), hierarchical micro/nanoporosity, and good electrical conductivity which could serve as a promising carbon material for advanced applications in energy, environmental, and biomedical fields.

1. Introduction

Owing to the ever growing energy demand, electrochemical energy storage systems with higher energy and power densities such as lithium-ion batteries (LIBs), supercapacitors (SCs), etc. have attracted tremendous attention [1,2]. In recent years, electrochemical supercapacitors have received a great interest as a renowned power sources because of their advantages of high power density coupled with extended cycle life, simple configuration, and easy mode of operation [3–7]. Although, electrochemical supercapacitors are widely used for numerous portable applications in the field of electronics, power backup, memory systems, etc. and they face tough challenges for producing high energy density supercapacitors in comparison to batteries [8,9]. In an effort to improve the energy density, nanostructured carbon based electrodes have played a major role among various electrode materials due to its low-cost, high electrical conductivity, and good durability. Generally, carbonaceous materials with high porosity and large surface area (1000–1500 m^2/g) deliver the energy density of ~5.0 Wh kg^{-1} and gravimetric capacitance of ~120.0 F g^{-1}. In this context, several carbon nanostructures such as graphene [10,11], carbon nanotubes [12,13] and carbon nanofibers [14,15] having a high surface area of ≥1500.0 $m^2 g^{-1}$ were investigated for supercapacitor applications. However, the forbidden production cost and attaining high pure material still remain a challenging task towards commercialization. Thus, the recent research efforts were widely focussed on the carbon based/derived materials having advantageous attributes like tuneable pore size, high surface area, low cost, and environmental benignity [16–18].

In search for better carbonaceous materials, activated carbons derived from various natural sources, food waste, bio wastes, etc. have been investigated extensively to find suitable carbon materials [19]. Impressed with low cost factor, high surface area, and environmental sustainability, biomass derived activated carbon materials are exceptionally attractive for energy storage applications [20]. While chemical etching approach is often used to prepare porous activated carbon through etching of metal or silica present in the metal organic framework (MOF) [21,22] the method generally involves multistep synthesis and unfriendly etching process. In this context, synthesis of biomass derived activated carbon is considered as a cost effective strategy where the presence of biomolecules create numerous pores on the carbon surface during high temperature activation [19,23]. Natural raw materials, including banana peel [24], human hair [25], corncobs [26],

* Corresponding author.
** Corresponding author.
E-mail addresses: maduraiveeran.g@ktr.srmuniv.ac.in (G. Maduraiveeran), sasidharan.m@res.srmuniv.ac.in (M. Sasidharan).

https://doi.org/10.1016/j.micromeso.2018.08.006
Received 6 May 2018; Received in revised form 19 July 2018; Accepted 6 August 2018
Available online 07 August 2018

teakwood sawdust [27], coir pith [28], rice husks [23], etc. [29–33] have been used to obtain the porous activated carbons materials using various chemical activation agents [34–40]. Therefore, developing a simple synthetic strategy using abundance low-cost precursors for the production of porous structured carbon nanomaterials with high surface area still remains a mainstream research.

Herein, we demonstrate for the first time a facile, cost-effective, and template-free large scale synthetic strategy for novel hierarchical CN material from food waste of Indian Cake Rusk (ICR) for application in high performance supercapacitor. The prime advantages of this study includes (i) a facile and effective synthetic strategy; (ii) high surface to volume ratio, economic and inexpensive sustainable resource of food waste as the precursor; (iii) high porosity with an average pore diameter of ~3 nm without using any template agents; (iv) can be integrated either as three-electrode or two-electrode configurations towards super capacitance application and (v) exhibits the best maximum energy density of 47.1 Wh kg^{-1} and power density of 22644.0 W kg^{-1} due to synergistic effect arising from large surface area and hierarchical nanoporous structure. The present investigation will endow with new opportunity for the large-scale production of highly mesoporous NAC from biomass for stimulating environmental and energy applications.

2. Experimental section

2.1. Synthesis of CN materials

In a typical synthesis of carbon material, the collected Indian Cake Rusk (ICR) food waste from Bakery was ground well using mortar and pestle to obtain a fine powder. The powder was then annealed in an alumina crucible at 450 °C for 4.0 h using a tubular furnace (Carbolite furnace, UK) under N_2 atmosphere at a ramp rate of 5 °C min^{-1} and the resultant carbon powder was collected after cooling down the furnace to room temperature. In order to activate the obtained carbon, it was mixed well with KOH (Alfa Aesar) in a stoichiometric ratio of 1:3. Finally, the mixed powder was transferred to an alumina crucible and again annealed at 750 °C for 3 h in an inert atmosphere. After cooling the furnace, the carbon material was collected, washed thoroughly with pure water till the combined washings attain pH ~7.0. Finally, the activated carbon material was collected by centrifugation and dried at 60 °C for overnight in a hot air oven.

2.2. Physiochemical characterization

Powder X-ray diffraction (XRD) pattern was recorded with a Philips XRD 'X'PERT PRO diffractometer with Cu K_α rays (λ = 1.5418 Å). FT-IR spectrum was carried out with a BRUKER OPTIK spectrometer, GMBH, Germany (Model No. TENSOR 27) using KBr pellet technique. Raman measurements were performed using Renishaw (UK) spectrometer with a incident wavelength laser light of 632.8 nm. Surface area measurements were performed with autosorb IQ series (Quantachrome Instruments). Field emission scanning electron microscopic (FESEM) measurement was accomplished using of FEI Quanta FEG 200 HR-SEM after coating desired carbon samples on sample stub and transmission electron microscopic (TEM) images were recorded with a JEOL (JEM-2100 Plus) operating at 200 kV by coating test carbon sample on a copper grid.

2.3. Electrochemical characterization

High-pure stainless steel foil with a thickness of 0.04 mm (SS 304, Alfa Aesar) was thoroughly polished with a emery paper followed by washing with pure water and acetone, and subsequently dried up in an oven at 60 °C for 3 h. The working electrodes were constructed by modifying the foil (geometrical surface area of ~1.0 cm^2) with slurry containing 85 wt% of as-synthesized porous activated carbon, 10 wt% of Super P carbon (Alfa Aesar) and 5 wt% of polyvinylidene difluoride (PVDF) (Alfa Aesar) in N-methyl-2-pyrrolidone solvent (NMP) (Alfa Aesar) and then dried at 120 °C under vacuum for 12 h. The mass of the active electrode materials was calculated to be ~1.2 mg/cm^2. The electrochemical properties were evaluated in a three-electrode configuration by using platinum (Pt) as a counter electrode, saturated calomel electrode (SCE) as a reference electrode and 1 M H_2SO_4 as an electrolyte in the potential window of −0.3 − 0.9 V. Whereas coin type symmetrical supercapacitor was assembled in an argon-filled glove box (M'BRAUN, Germany) with < 1.0 ppm of oxygen and moisture content. $LiPF_6$ salt dissolved in EC:DMC solvents (1:1 vol%) was used as an electrolyte and polypropylene was used as a separator in symmetrical supercapacitors. Electrochemical measurements were performed in the potential window of 0.0–2.5 V using a Biologic workstation (VSP-300). The electrochemical impedance spectroscopic (EIS) measurement was performed in the frequency range of 10 mHz–100 kHz. Discharge specific capacitance (SC) of the activated porous carbon material was estimated by means of the following equation for three electrode system:

$$SC = I\,t / (m\,\Delta V) \quad (1)$$

And the specific energy (SE) and specific power (SP) of a supercapacitor were estimated using the following equations [41,42].

$$SE = (It\Delta V/m)/2 \quad (2)$$

$$SP = (I\Delta V/m)/2 \quad (3)$$

Where, "*I*" refers the current in ampere used for charge/discharge cycling, "t" presents the time required for discharge, "m" means the mass in grams of the active carbon material and "*ΔV*" is the operating potential window in 'volt' for the charge or discharge. Discharge specific capacitance (SC) value of the porous activated carbon electrode for two electrode system was measured using the following equation [43]:

$$SC = 4\ I\ t/m\Delta V \quad (4)$$

The values of energy density and power density for the as-developed activated porous carbon (NAC) material were estimated using the following equation [44,45],

$$\text{Energy density} = 1/2C * \Delta V^2 * 1/3.6 \quad (5)$$

$$\text{Power density} = E/\Delta t*3600 \quad (6)$$

Where, "C" represents the specific capacitance, "*ΔV*" refers the potential window, "*E*" presents the energy density and "t" the discharge time in seconds.

3. Results and discussion

As a class of biomass, ICR mainly contains wheat flour which has high surface area, large surface to volume ratio, and huge porosity. Schematic representation for the synthesis NAC material from food waste of ICR is presented in Scheme 1. The hierarchical nanoporous activated carbon material was produced without using any sacrificial templates simply by thermal annealing (carbonization) and followed by chemical activation process at 750 °C. Fig. 1a shows the X-ray diffraction patterns of the NAC materials obtained prior to- and after KOH activation process, indicating a low degree of crystallinity. The characteristic diffraction peaks observed at 25.0 and 43.0 2θ corresponding to (002) and (100) planes indicate a typical layered structure with short-range order. As shown in Fig. 1a, the crystallinity of the NAC

Scheme 1. Schematic illustration of the synthesis of the NAC materials.

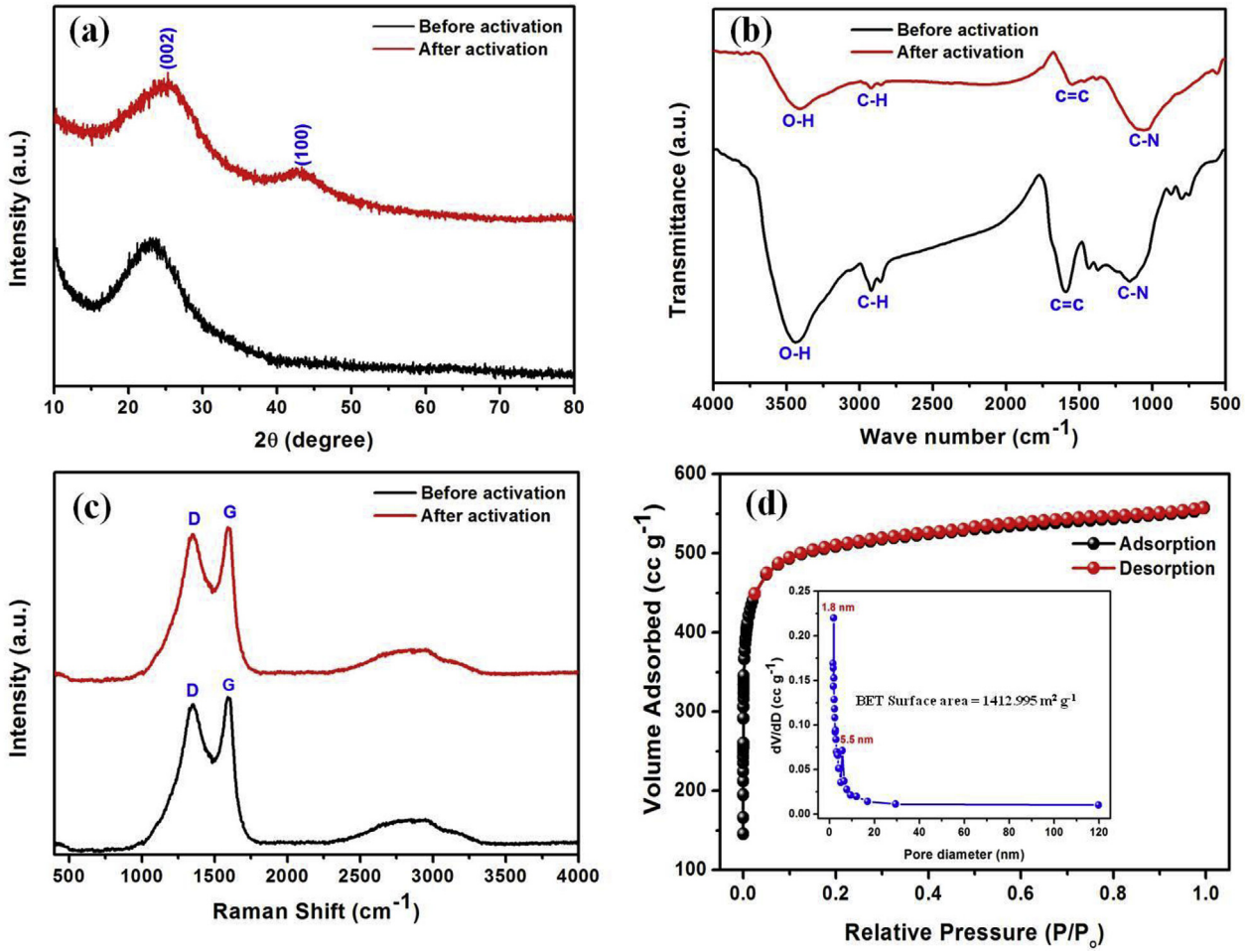

Fig. 1. (a) Powder X-ray diffraction patterns of NAC material prior to- (black curve) and after activation (red curve); (b) FT-IR spectra of the developed NAC material prior to- (black curve) and after activation (red curve); (c) Raman spectra of the developed NAC material prior to- (black curve) and after activation (red curve); (d) BET N_2 adsorption-desorption isotherm of NAC material (Inset: The corresponding pore size distribution profile). (For interpretation of the references to colour in this figure legend, the reader is referred to the Web version of this article.)

materials is improved after KOH treatment due to encryption of ordered nanoporous structure on the NAC materials at high temperature treatment. The nature of functional groups present on the carbon surface was identified with the help of FTIR spectroscopy. Fig. 1b shows the FTIR spectra of the NAC developed before and after KOH activation process clearly exhibiting the presence of functional groups such as −OH, −CH, −C=C−, −CN, etc. The characteristic peak for O−H stretching frequency was centered at 3438.0 cm^{-1} for the unactivated carbon samples, which had shifted to 3409.0 cm^{-1} after KOH activation process. The C−H and C=C stretching frequency were also observed at ~2922.0 cm^{-1} and ~1590.0 cm^{-1} for both the materials indicating moderate graphite like extended conjugation. Furthermore, the existence of −C≡N group on carbon matrix might be originated from N-containing biomass constitutents.

The Raman spectra of the developed NC material before and after KOH activation are shown in Fig. 1c. The resonance peaks observed at 1348.0 cm^{-1} and 1590.0 cm^{-1} for both raw and activated materials show characteristic D and G bands. In addition, the presence of D band (defects) in the graphitic lattice represent the A_{1g} symmetry while the existence of single crystalline carbon atoms in the sp^2 hybridization of the layered graphitic structure show E_{2g} mode.[46] The G band intensity is relatively higher than that of D band intensity representing an enhancement of the graphitic structure with fewer defect sites in the NAC materials than of the corresponding materials without KOH activation [47]. In order to evaluate textural properties such as porosity, pore volume, and BET surface area, the NAC material and prior activation material was subjected to nitrogen adsorption-desorption measurements (Fig. 1d). The N_2 isotherm was found to be typical Type I isotherm according to IUPAC classification. The BET surface area of NAC material was found to be 1413.0 $m^2 g^{-1}$ with a pore volume of 0.737 $cm^3 g^{-1}$ which is significantly higher (~24 times) than that of carbon material prior to KOH activation (surface area (58.0 $m^2 g^{-1}$)). Furthermore, the shape of nitrogen adsorption/desorption isotherm indicate that majority of pores are micropores with small portion of mesopores. It is presumed that the release of high gaseous product during KOH activation process is the key factor to achieve high surface area porous carbon compared to prior to activation sample and also there is no change in crystal structure for the both samples which is evident by XRD (Fig. 1a), the enhance the electrochemical performance is mainly due to the huge surface area and porosity of the NAC material. The electrolyte ions transportation is mainly determined by porosity, pore size of the material, such pores are considered to be beneficial for the fast movement of ions between the electrolyte and the active material to obtain enhanced electro kinetics. Pore size distribution curve further shows (Fig. 1d, inset) that non-uniform mesopores with diameter in the range of ~1.8 nm–~5.5 nm located in the NAC. The value of apparent density was also calculated as 0.61, 0.45, 0.04 and 0.12 kg/m^3 for graphite, graphene, single walled carbon nanotubes and NAC material, respectively. A NAC material with mesopores and micropores well-distributed, which permits active ions in the micropores results shortening the transportation time and low-resistant ion transport paths more favorable ideal for EDLCs. Thus the combination of microporous,

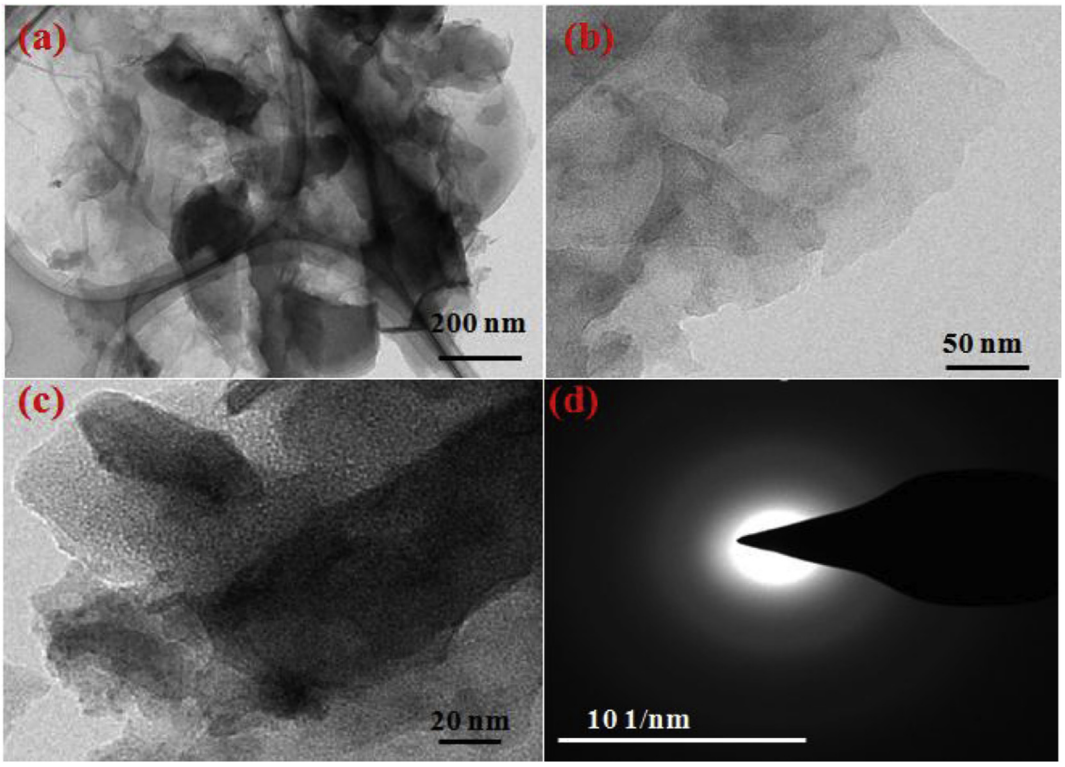

Fig. 2. (a–c) TEM images and (d) SAED pattern of the NAC material.

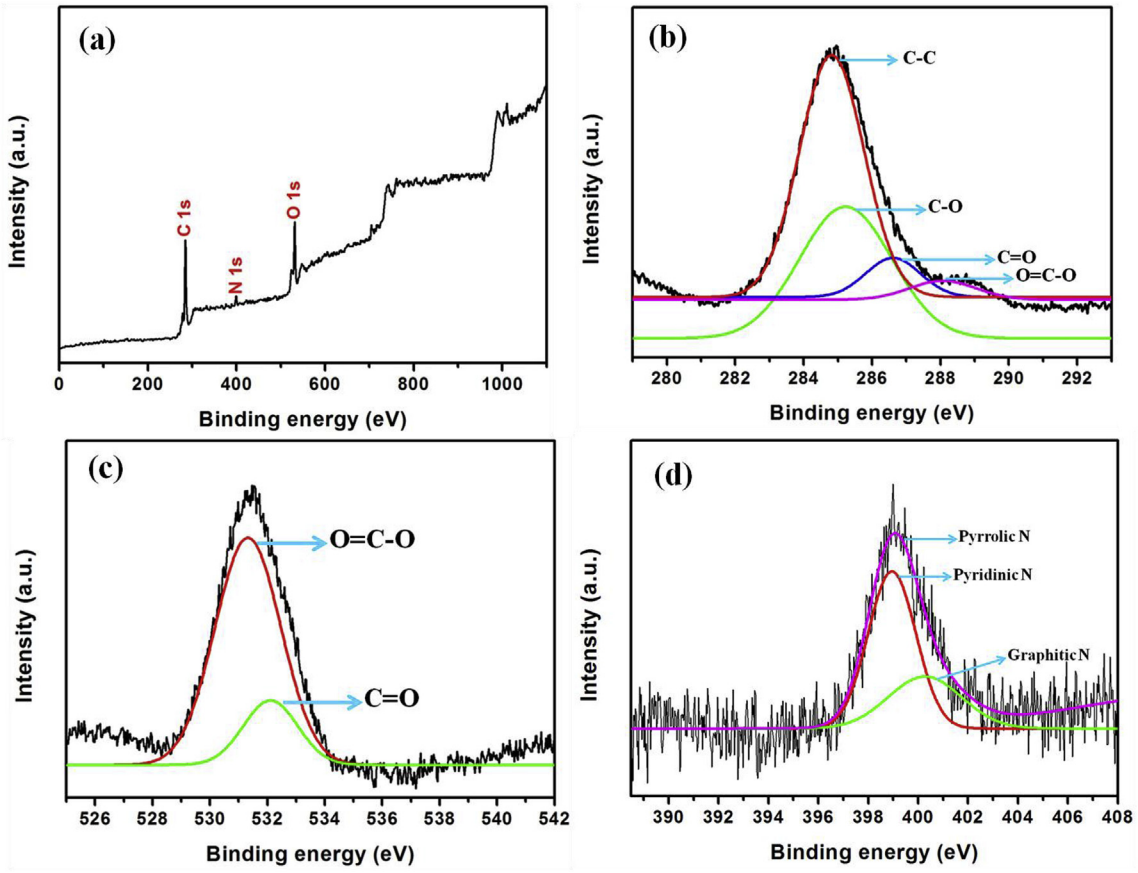

Fig. 3. XPS spectra of (a) survey scan, (b) C 1s, (c) O 1s and (d) N 1s of the NAC material.

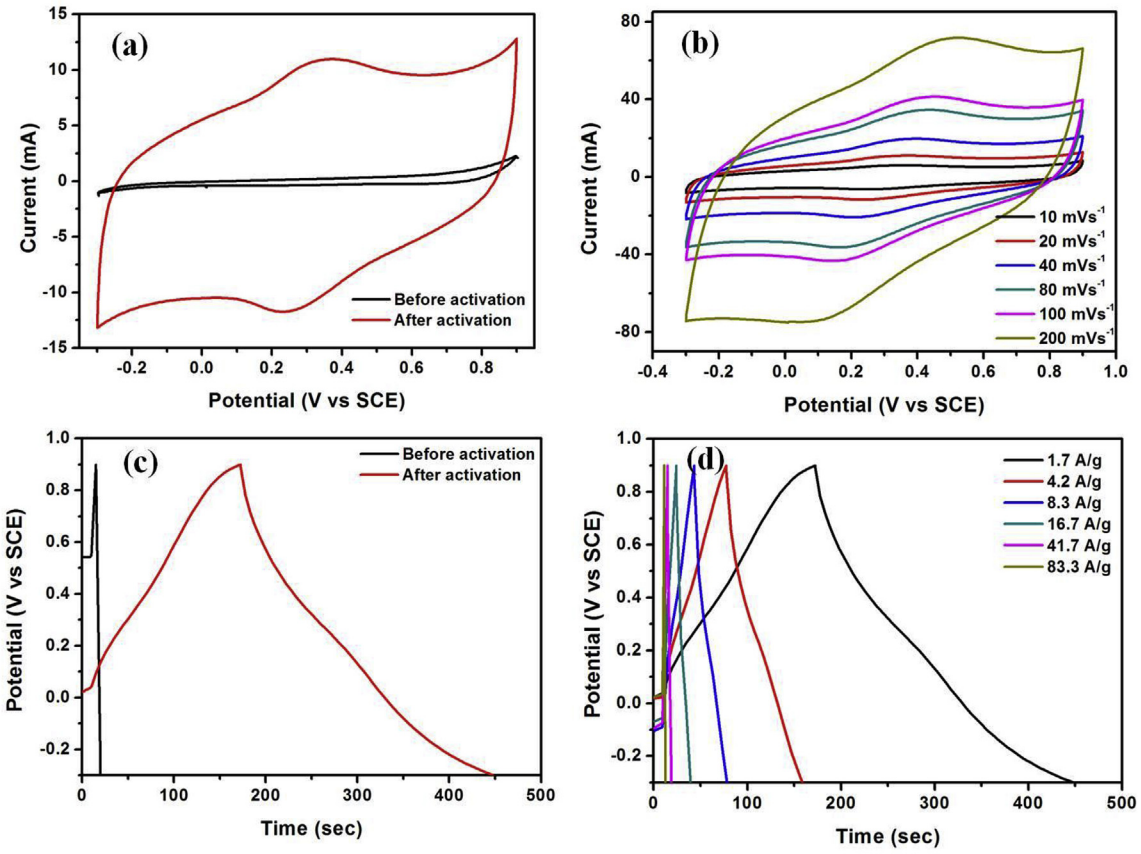

Fig. 4. (a) CVs of the NAC electrode prior to- (black curve) and after activation (red curve) at a scan rate of 20 mV s^{-1} (b) CVs of the NAC electrode at various scan rates. (c) Galvanostatic charge-discharge profile of the NAC electrode prior to- (black curve) and after activation (red curve) at a current density of 1.7 A/g. (d) Galvanostatic charge-discharge profile of the NAC electrode at different applied current densities. (For interpretation of the references to colour in this figure legend, the reader is referred to the Web version of this article.)

Table 1
Comparing the performance of various bio-waste based NAC electrode used for supercapacitor applications.

S.No	Carbon Source	Specific Capacitance (F g^{-1})	Current density (A g^{-1})	Electrolyte	Cycle Life	Energy Density (Wh kg^{-1})	Power Density (W kg^{-1})	Ref.
1	Rice husk	147.0	0.1	6M KOH	10000	5.11	–	[52]
2	Rice bran	265.0	10.0	6M KOH	10000	70.0	1223.0	[53]
3	Bagasse waste	320.0	0.5	1M Na_2SO_4	15000	20.0	182.0	[54]
4	Bamboo char	222.0	0.5	6M KOH	5000	20.6	12000.0	[55]
5	Food waste	106.0	1.0 mA	3M KOH	500	–	–	[56]
6	Waste tea	203.0	1.5 mA	1M H_2SO_4	400	–	–	[57]
7	Carton box	311.0	0.5	6M KOH	5000	10.8	125.0	[58]
8	Waste tire	106.0	1.0	6M KOH	1000	–	–	[59]
9	Lignin	312.0	1.0	6M KOH	20000	44.7	–	[60]
10	Puffed rice	334.0	0.5	6M KOH	11000	104.0	–	[61]
11	**ICR**	**381.0**	**1.7**	**1M H_2SO_4**	**6000**	**-**	**-**	**This work**
		217.0	**0.35**	**1M $LiPF_6$**	**10000**	**47.1**	**22644.0**	

mesoporous textural features coupled with high BET surface would be anticipated to enhance electrochemical performance such as specific capacitance, cycle life stability, energy density, and power density.

The surface morphology of the NAC was investigated with TEM and FESEM techniques. Further confirmation of various elements present in the porous carbon was obtained by EDAX (Fig. S1). The elemental analysis confirms the presence of C, O and N in the NAC. Fig. 2a–c presents the TEM images of the NAC and average mesopore size was calculated to be ~3.0 nm, respectively. Interestingly, nanoporous structures were also heavily dispersed with a uniform distribution as displayed in Fig. 2c and Fig. S2. Fig. 2d shows a typical selected area electron diffraction (SAED) pattern of the NAC. The SAED diffuse ring patterns appeared without any bright spots, revealing the polycrystalline nature of the NAC as observed from the XRD pattern (Fig. 1a).

The XPS measurements were also performed to characterize the surface elemental composition of the NAC material. As shown in Fig. 3a, the XPS survey spectra confirmed the presence of C, O, and N in the NAC material. Fig. 3b shows the XPS spectra of C 1s which showed four-peaks located at ~284.8, ~285.2, ~288.6 and ~288.2 eV, corresponding to the presence of sp^2 hybridized C—C, C—O, C=O, and O=C—O groups. Further, O 1s spectrum of Fig. 3c depicts two-peaks located at ~531.3 and ~532.1, due to the presence of different oxygen functional groups of O=C—O and C=O groups. Fig. 3d displays the N 1s spectra showed three-peaks which are located at ~398.9, ~399.2, and ~400.3 eV, corresponding to the presence nitrogen functionalities such as pyridinic-N, pyrrolic-N and graphitic N. These results clearly reveal that the developed NAC material also possessed the nitrogen species as evidenced in the FTIR (Fig. 1b) and EDAX (Fig. S1) studies.

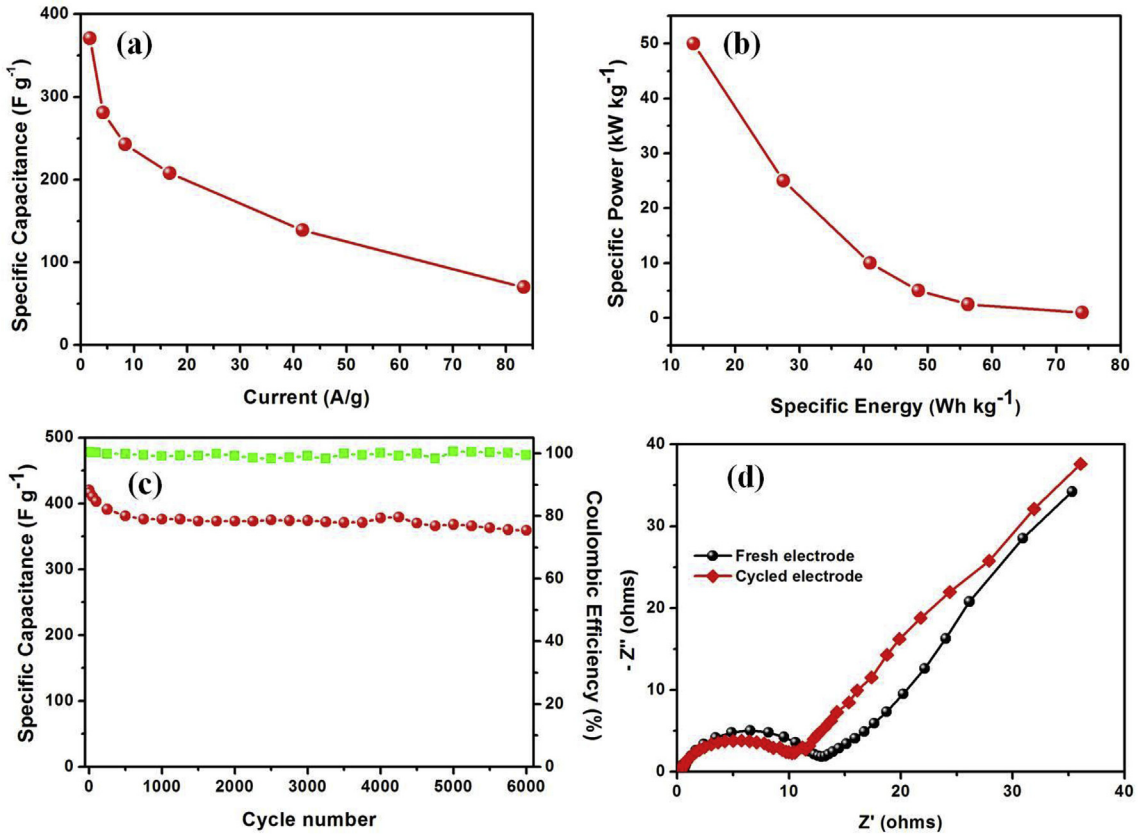

Fig. 5. (a) Dependence of specific capacitance on various current densities and (b) Ragone plot of the NAC electrode in three electrode system. (c) Cycle life of the NAC electrode recorded at a current density of 1.7 A/g. (d) EIS spectra of fresh (block curve) and after cycled NAC electrode (red curve). (For interpretation of the references to colour in this figure legend, the reader is referred to the Web version of this article.)

The presence of nitrogen in the NAC material could play a major role on the enhancement of the electronic conductivity and pseudo-capacitive characteristics [32,46,48,49].

The electrochemical supercapacitive performance of the NAC was investigated using cyclic voltammetric (CV) and galvanostatic charge-discharge studies both in three-electrode system using aqueous 1.0 M H_2SO_4 electrolyte and two-electrode set-up with non-aqueous electrolyte containing 1.0 M $LiPF_6$ salt. In the three-electrode system, the electrochemical supercapacitance study was performed in the operating potential window from −0.3 to 0.9 V *vs* SCE in 1.0 M H_2SO_4. Fig. 4a shows the CV curves of NAC constructed electrode before (black curve) and after activation (red curve) at a scan rate of 20 mV s^{-1}. The rectangular shape of voltammogram revealed an ideal electrochemical double layer capacitance (EDLC) behavior for carbons both before and after activation step. Nevertheless, the pseudo-capacitive behavior was also observed in the potential range of 0.1–0.4 V which may be caused due to the presence of heteroatoms (nitrogen) on the surface of carbon materials as evidenced from FTIR (Fig. 1b), EDAX (Fig. S1), and XPS (Fig. 3d). As expected, the KOH activated NAC exhibited higher capacitance compared to unactivated carbon sample as shown in Fig. 4a. Huge surface area coupled with nano-macro pore architecture of NAC perhaps help high charge storage as seen from the area of CV curve in Fig. 4a. Fig. 4b depicts the CV curves of the NAC recorded in 1.0 M H_2SO_4 electrolyte at various scan rates varying from 10.0 mV s^{-1} to 200.0 mV s^{-1}. The rectangular shape of the CVs exhibited a replicate image of cathodic and anodic parts, confirming the ideal capacitive behavior. The voltammograms of the present NAC materials also indicated monotonically increasing peak current with rise of scan rate as displayed in Fig. S2. It is noteworthy to mention that even at higher scan rates the characteristic rectangular feature remains very stable, thus demonstrating a superior rate capability and reversibility of the ICR-derived carbon electrodes. The surface adsorption-desorption properties of the present system obtained from Fig. S3, showed a near linearity due to the non-Faradaic surface adsorption-desorption process over the porous carbon electrode [50,51]. As shown in Fig. S4, the synthesized NAC materials exhibited higher double layer capacitive behavior in comparison to other carbon materials such as graphite, graphene, and single walled carbon nanotubes, due to the ascription of high electrochemical active surface area of NAC material.

The typical galvanostatic charge-discharge (CD) study was also used to investigate the capacitive behavior of the developed NAC materials. Fig. 4c shows a typical EDLC behavior of the NAC electrodes before (black curve) and after (red curve) the KOH activation process using aqueous 1.0 M H_2SO_4 electrolyte at an applied current density of 1.7 A g^{-1}. The unactivated carbon material showed a linear CD curve with a lower specific capacitance of 28.0 F g^{-1} at a current density of 1.7 A g^{-1}. However, the NAC electrode (red curve) exhibited a slightly non-linear behavior with time, exhibiting two plateaus, one during the charging (~0.35 V) and other at discharging (~0.23 V) process possibly due to the presence of heteroatoms on the surface of carbon electrodes [32] as observed in the CD curves of Fig. 4c and Fig. S3. Thus, the present NAC electrode exhibited a high specific capacitance of 381.0 F g^{-1} at a current density of 1.7 A g^{-1} which is more than ~10.0 times higher than that of the corresponding unactivated carbon as depicted in Fig. 4c. The impressive specific capacitance of the present NAC electrode is ascribed to their high surface area, hierarchical interconnected micro/nano-pores and facile electrode kinetics and the performance of present NAC surpass the previous reports on supercapacitors using biomass-based carbon electrodes as shown in Table 1.

In order to further understand the rate capability of ICR-derived NAC electrode, the charge-discharge profiles were recorded at different current densities ranging from 1.7 A g^{-1} to 83.3 A g^{-1} (Fig. 4d). The

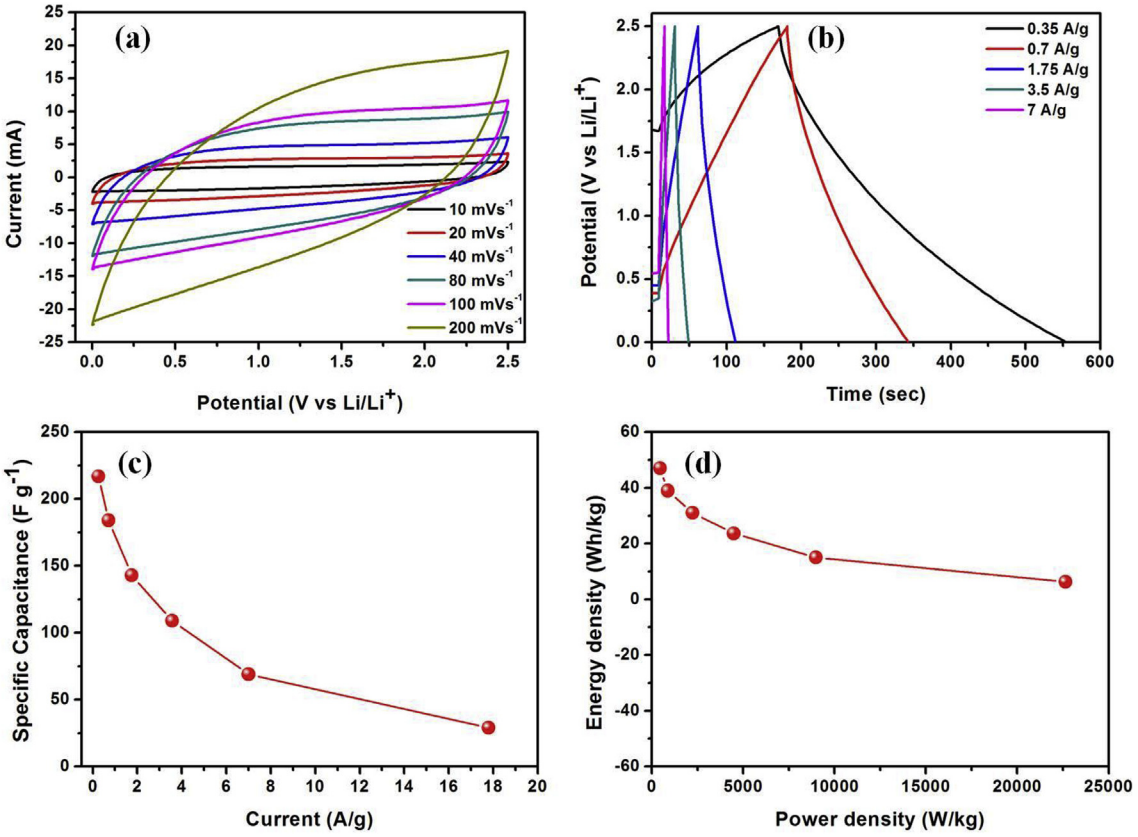

Fig. 6. (a) CVs of the NAC electrode recorded in 1.0 M $LiPF_6$ as an electrolyte at different scan rates. (b) Galvanostatic charge-discharge profile of NAC electrode at different current densities. (c) Specific capacitance as a function of different current density and (d) Ragone plot of the NAC in two electrode system.

specific capacitance values of the present electrode were calculated to be 381.0, 281.0, 243.0, 208.0, 139.0, and 70.0 F g^{-1} at applied constant current densities of 1.7, 4.2, 8.3, 16.7, 41.7, and 83.3 A g^{-1}, respectively as presented in Fig. 5a. It is seen that the specific capacitance was decreased from 381.0 F g^{-1} to 70.0 F g^{-1} by increasing the current density probably due to pulverization of active materials at higher current density [41,62]. For any practical applications, both energy density and power density are two central factors. Fig. 5b shows the Ragone plot of the carbon electrode under present investigation, where the specific energy decreases with the increasing specific power exhibiting a typical supercapacitor behavior. The specific energy values were 74.0, 56.3, 48.5, 41.0, 27.5, and 13.5 Wh kg^{-1} corresponding to the specific power values of 1.0, 2.5, 5.0, 10.0, 25.0, and 50.0 kW kg^{-1}, respectively, which are higher in comparison to the formerly reported values using NAC material obtained from different sources (Table 1). The improved specific power of the developed NAC electrode is solely attributed to the high specific capacitance and cell voltage.

To operate supercapacitors for high power applications, cycle life is one of the major detrimental electrode properties. In this context, to investigate the stability and durability of the as-developed NAC electrode, cycle life study was performed by subjecting to a constant applied current density of 1.7 A g^{-1} and the data is shown in Fig. 5c. The specific capacitance of the carbon electrode under scrutiny was slightly decreased to 381.0 F g^{-1} from 422.0 F g^{-1} after performing continuous 250.0 cycles and thereafter, the specific capacitance (381.0 F g^{-1}) was maintained at the same level for over 6000 cycles as presented in Fig. 5c. The capacity retention and columbic efficiency were found to be more than 95.0% and ~99.5%, respectively, demonstrating a superior electrochemical performance and excellent durability of the developed NAC electrode in the present study. Fig. 5d shows the Nyquist plots of fresh and cycled NAC electrodes. The Nyquist plots show semicircle at high and middle frequency region and a linear slope at the low frequency region representing the contributions from the solution resistance (R_s), charge transfer resistance (R_{ct}) and diffusion kinetics. In the high frequency region, low solution resistance was observed for cycled NAC electrode when compared to the corresponding fresh NAC electrode, showing high electronic conductivity. At the low frequency region, the value of R_{ct} was significantly decreased to 10.4 Ω from 18.0 Ω after cycling for 6000 cycles due to its improved electronic conductivity. As depicted in Fig. 5d, the Warburg line also confirmed the double layer capacitance behavior and ionic diffusion at the electrode and electrolyte interface [61].

Furthermore, the ICR-derived NAC electrode was also investigated for symmetrical supercapacitors using non-aqueous electrolyte containing 1.0 M $LiPF_6$ salt dissolved in ethylene carbonate/dimethyl carbonate solvents (EC:DMC, 1:1 vol rato). It is widely recognized that a broad working voltage window is required in order to enhance the energy density as in the case of non-aqueous electrolyte with symmetrical supercapacitors [63–65]. The CVs of the NAC electrode were recorded in the voltage window of 0.0–2.5 V at different scan rates from 10.0 mV s^{-1} to 200.0 mV s^{-1} (Fig. 6a). The NAC electrode displayed a rectangular voltammogram feature irrespective of the applied scan rate as shown in Fig. 6a. As the scan rate increases, current density was also increased linearly, implying a surface adsorption-desorption process of the NAC electrode similar to results obtained with an aqueous electrolyte (Fig. S5). Fig. 6b presents the galvanostatic charge-discharge profiles of the carbon electrode by applying various current densities starting from 0.35 A g^{-1} to 17.8 A g^{-1}. The symmetrical supercapacitive characteristics of the NAC electrode are also in good agreement with double layer supercapacitor shown in Fig. 4. As displayed in Fig. S6, the NAC demonstrated a specific capacitance of 217.0 F g-1 at a current density of 0.35 A g^{-1}. Furthermore, the NAC electrode exhibited specific capacitances of 217.0, 184.0, 143.0, 109.0, 69.0, and 29.0 F g-1 at the constant applied current densities of 0.35, 0.7, 1.75,

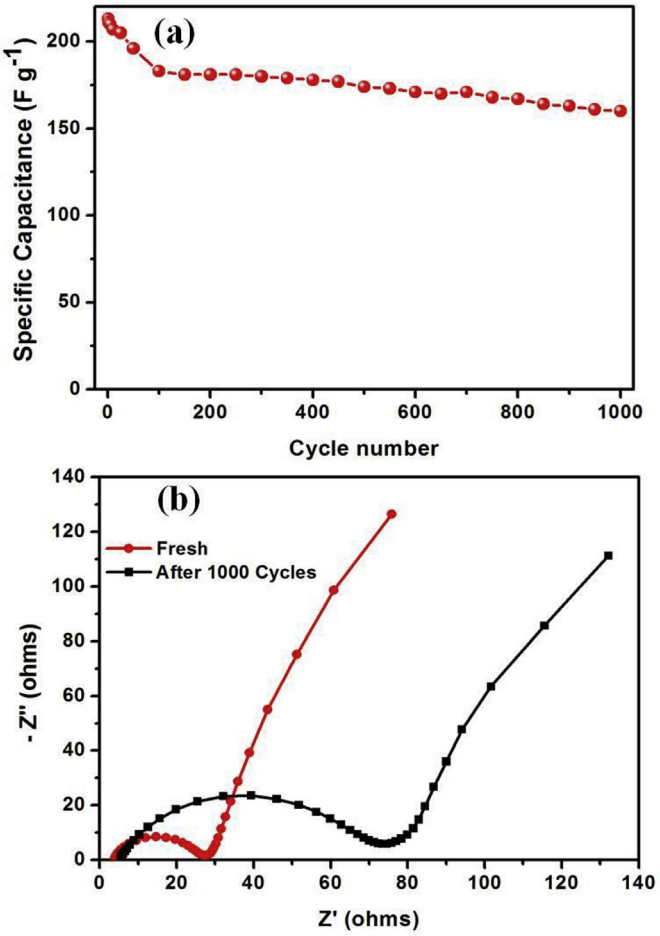

Fig. 7. (a) Cycle life of the NAC electrode at a current density of 0.35 A/g and (b) EIS spectra of the NAC electrode fresh (red curve) and after had a cycled electrode (black curve). (For interpretation of the references to colour in this figure legend, the reader is referred to the Web version of this article.)

3.57, 7.0, and 17.8 A g^{-1}, respectively (Fig. 6c).

Fig. 6d shows the Ragone plot of the NAC electrode. The values of energy density and power density of the ICR-derived NAC electrode were 47.1, 38.9, 31.0, 23.7, 15.0, and 6.3 Wh kg^{-1}; and 446.1, 870.5, 2234.2, 4481.1, 8982.0 and 22644.0 W kg^{-1}, respectively. The NAC electrode demonstrated a maximum energy density and power density of 47.1 Wh kg^{-1} and 22644.0 W kg^{-1}, respectively. It is observed that two electrode systems using non-aqueous electrolyte achieved a higher energy density and power density when compared to the three-electrode system with an aqueous electrolyte because of its high operating potential window. It is remarkable that the present biomass derived NAC delivered a maximum energy density of 47.1 Wh $kg^{-1}$and power density also increased to 8982.0 W kg^{-1} at an energy density of 15.0 Wh kg^{-1}. The superior supercapacitance performance of present NAC also compared with the reported biomass based carbon electrode materials as shown in Table 1. The significantly improved performance of the NAC electrode is ascribed to the following factors: (i) the synthesized nanoporous-structured carbon materials may offer beneficial physiochemical properties such as huge surface area of 1413.0 $m^2 g^{-1}$, hierarchical porous structure with a pore volume of 0.737 $cm^3 g^{-1}$, elevated electronic conductivity (R_{ct}: 27.5 Ω) and high apparent density of 0.12 kg/m^3; (ii) The NAC materials may afford more accessible active sites and adsorption on double sides, facilitating high performance electrochemical characteristics; and (iii) the design of two electrode symmetrical electrochemical storage system with NAC electrode in a wide voltage window (Fig. 6). The porous-structured 2-D materials highly permits active ions in the micropores, results shortening the transportation time and low-resistant ion transport paths more favorable ideal for EDLCs [30,32,33].

Fig. 7a shows the long-term cycle life study of the NAC electrode over 1000 cycles at a current density of 0.35 A g^{-1}. The initial specific capacitance of the NAC electrode was ~213.0 F g^{-1} which gradually decreased to 160.0 F g^{-1} upon continuous cycling of the electrode. About 75.0% retention of the specific capacitance was attained at the NAC electrode and lower retention is ascribed to decomposition of the electrolyte in the two electrode system. Fig. 7b shows the Nyquist plot of the NAC in symmetrical two electrode system. Semicircle present at higher frequency region (R_{ct}) of the cycled electrode was high (75.0 Ω) in comparison to the fresh electrode (27.5 Ω). The electronic conductivity of the NAC electrode was decreased after running 1000 cycles which may be due to the decomposition of electrolyte during continuous cycling [66].

4. Conclusion

In summary, we have successfully developed a simple but effective template-free strategy for the large-scale synthesis of well-ordered nanoporous activated carbon material directly from food waste of ICR for application in high-performance supercapacitor. Activation of carbon materials played a critical role in enhancing the specific surface area, porosity vis-à-vis electrochemical performance. The as-developed NAC material possessed a high surface area of 1413.0 $m^2 g^{-1}$ than the corresponding inactivated carbon samples. The present NAC electrode delivered a high specific capacitance of 381.0 F g^{-1} at 1.7 A g^{-1} and showed a remarkable capacity retention with almost 100% columbic efficiency after 6000 charge-discharge cycles in 1.0 M H_2SO_4. ICR-derived NAC electrode also delivered a high energy density and power density of 47.1 Wh kg^{-1} and 22644 W kg^{-1}, respectively in 1.0 M $LiPF_6$ in symmetrical supercapacitor configuration. High porosity and huge surface area coupled with high electrical conductivities are reasoned for significant improvement in the supercapacitive performance. We strongly believe that the present study would offer a new prospect for fabrication of high-performance carbon based electrode materials with promising applications in fields of supercapacitor, battery, adsorption technology, and catalysis.

Acknowledgements

The authors acknowledge Ministry of New and Renewable Energy India, Govt. of India for financial assistance (No.31/03/2014-15/PVSE-R&D). T.K. thanks to Council of Scientific and Industrial Research for providing Senior Research Fellowship (SRF). The authors also thanks to DST-FIST (fund for improvement of S&T infrastructure) for financial assistance for Department of Chemistry, SRM Institute of Science and Technology, No.SR/FST/CST-266/2015(c).

Appendix A. Supplementary data

Supplementary data related to this article can be found at https://doi.org/10.1016/j.micromeso.2018.08.006.

References

[1] J.R. Miller, P. Simon, Electrochemical capacitors for energy management, Science 321 (2008) 651–652.
[2] S. Sarangapani, B.V. Tilak, C.P. Chen, Materials for electrochemical capacitors, J. Electrochem. Soc. 143 (1996) 3791–3799.
[3] B.E. Conway, Electrochemical Supercapacitors Scientific Fundamentals and Technological Applications, (1999) 978-1-4757-3058-6.
[4] S.S. Thind, X. Chang, J.S. Wentzell, A. Chen, High-performance supercapacitor based on tantalum iridium oxides supported on tungsten oxide nanoplatelets, Electrochem. Commun. 67 (2016) 1–5.
[5] Y. Ma, H. Chang, M. Zhang, Y. Chen, Graphene-based materials for lithium-ion hybrid supercapacitors, Adv. Mater. 27 (2015) 5296–5308.
[6] V. Aravindan, J. Gnanaraj, Y.S. Lee, S. Madhavi, Insertion-type electrodes for

nonaqueous li-ion capacitors, Chem. Rev. 114 (2014) 11619–11635.
[7] T. Abbasi, S.A. Abbasi, Decarbonization of fossil fuels as a strategy to control global warming, renewable, Sustain. Energy Rev. 15 (2011) 1828–1834.
[8] L.L. Zhang, X.S. Zhao, Carbon-based materials as supercapacitor electrodes, Chem. Soc. Rev. 38 (2009) 2520–2531.
[9] Q. Wang, J. Yan, Z. Fan, Carbon materials for high volumetric performance supercapacitors: design, progress, challenges and opportunities, Energy Environ. Sci. 9 (2016) 729–762.
[10] M.D. Stoller, S. Park, Y. Zhu, J. An, R.S. Ruoff, Graphene-based ultracapacitors, Nano Lett. 8 (2008) 3498–3502.
[11] S. Boopathi, A.R. Thiruppathi, A. Chen, From graphite to interconnected reduced graphene oxide: one-pot synthesis and supercapacitor application, Chem. Commun. 53 (2017) 7828–7831.
[12] R.H. Baughman, A.A. Zakhidov, W.A. De Heer, Carbon nanotubes-the route toward applications, Science 297 (2002) 787–792.
[13] H. Pan, J. Li, Y. Feng, Carbon nanotubes for supercapacitor, Nanoscale Res. Lett. 5 (2010) 654–668.
[14] K. Wang, Y. Wang, Y. Wang, E. Hosono, H. Zhou, Mesoporous carbon nanofibers for supercapacitor application, J. Phys. Chem. C 113 (2009) 1093–1097.
[15] Y. Liu, J. Zhou, L. Chen, P. Zhang, W. Fu, H. Zhao, Y. Ma, X. Pan, Z. Zhang, W. Han, E. Xie, Highly flexible free standing porous carbon nanofibers for electrodes materials of high-performance all-carbon supercapacitors, ACS Appl. Mater. Interfaces 7 (2015) 23515–23520.
[16] E. Frackowiak, F. Beguin, Carbon materials for the electrochemical storage of energy in capacitors, Carbon 39 (2001) 937–950.
[17] A.G. Pandolfo, A.F. Hollenkamp, Carbon properties and their role in supercapacitors, J. Power Sources 157 (2006) 11–27.
[18] E. Frackowiak, Carbon materials for supercapacitor application, Phys. Chem. Chem. Phys. 9 (2007) 1774–1785.
[19] J. Wang, P. Nie, B. Ding, S. Dong, X. Hao, H. Doua, X. Zhang, Biomass derived carbon for energy storage devices, J. Mater. Chem. A 5 (2017) 2411–2428.
[20] M.-X. Liu, L.-Y. Chen, D.-Z. Zhu, H. Duan, W. Xiong, Z.-J. Xu, L.-H. Gan, L.-W. Chen, Zinc tartrate oriented hydrothermal synthesis of microporous carbons for high performance supercapacitor electrodes, Chin. Chem. Lett. 27 (2016) 399–404.
[21] O. Fleker, A. Borenstein, R. Lavi, L. Benisvy, S. Ruthstein, D. Aurbach, Preparation and properties of metal organic framework/activated carbon composite materials, Langmuir 32 (2016) 4935–4944.
[22] M.-H. Kim, K.-B. Kim, S.-M. Park, K.C. Roh, Hierarchically structured activated carbon for ultracapacitors, Sci. Rep. 6 (2016) 21182.
[23] C. Kunfeng, X. Dongfeng, Multiple functional biomass-derived activated carbon materials for aqueous supercapacitors, lithium-ion capacitors and lithium-sulfur batteries, Chin. J. Chem. 35 (2017) 861–866.
[24] V. Subramanian, C. Luo, A.M. Stephan, K.S. Nahm, S. Thomas, B. Wei, Supercapacitors from activated carbon derived from banana fibers, J. Phys. Chem. C 111 (2007) 7527–7531.
[25] K.R. Saravanan, N. Kalaiselvi, Nitrogen containing bio-carbon as a potential anode for lithium batteries, Carbon 81 (2015) 43–53.
[26] B. Li, F. Dai, Q. Xiao, L. Yang, J. Shen, C. Zhang, M. Cai, Nitrogen-doped activated carbon for a high energy hybrid supercapacitor, Energy Environ. Sci. 9 (2016) 102–106.
[27] A. Jain, S. Jayaraman, U. Ulaganathan, R. Balasubramanian, A. Aravindan, M.P. Srinivasan, S. Madhavi, Highly mesoporous carbon from teak wood sawdust as prospective electrode for the construction of high energy li-ion capacitors, Electrochim. Acta 228 (2017) 131–138.
[28] V. Mullaivananathan, R. Sathish, N. Kalaiselvi, Coir pith derived bio-carbon: demonstration of potential anode behavior in lithium-ion batteries, Electrochim. Acta 225 (2017) 143–150.
[29] L. Sun, C. Tian, M. Li, X. Meng, L. Wang, R. Wang, J. Yin, H. Fu, From coconut shell to porous graphene-like nanosheets for high-power supercapacitors, J. Mater. Chem. A 1 (2013) 6462–6470.
[30] M. Xu, T. Liang, M. Shi, H. Chen, Graphene-like two-dimensional materials, Chem. Rev. 113 (2013) 3766–3798.
[31] S. Ucar, M. Erdem, T. Tay, S. Karagoz, Preparation and characterization of activated carbon produced from pomegranate seeds by $ZnCl_2$ activation, Appl. Surf. Sci. 255 (2009) 8890–8896.
[32] M. Karnan, K. Subramani, N. Sudhan, N. Ilayaraja, M. Sathish, Aloe vera derived activated high-surface-area carbon for flexible and high-energy supercapacitors, ACS Appl. Mater. Interfaces 8 (2016) 35191–35202.
[33] C. Zhan, X. Yu, Q. Liang, W. Liu, Y. Wang, R. Lv, Z.-H. Huang, F. Kang, Flour food Waste derived activated carbon for high-performance supercapacitors, RSC Adv. 6 (2016) 89391–89396.
[34] J. Yan, Q. Wang, T. Wei, Z. Fan, Supercapacitors: recent advances in design and fabrication of electrochemical supercapacitors with high energy densities, Adv. Energy Mater 4 (2014) 1300816.
[35] J. Hayashi, A. Kazehaya, K. Muroyama, A.P. Watkinson, Preparation of activated carbon from lignin by chemical activation, Carbon 38 (2000) 1873–1878.
[36] M.S. Solum, R.J. Pugmire, M. Jagtoyen, F. Derbyshire, Evolution of carbon structure in chemically activated wood, Carbon 33 (1995) 1247–1254.
[37] D. Hulicova-Jurcakova, A.M. Puziy, O.I. Poddubnaya, F. Suárez-García, J.M.D. Tascón, G.Q. Lu, Highly stable performance of supercapacitors from phosphorus-enriched carbons, J. Am. Chem. Soc. 131 (2009) 5026–5027.
[38] P. Cheng, T. Li, H. Yu, L. Zhi, Z. Liu, Z. Lei, Biomass-derived carbon fiber aerogel as a binder-free electrode for high-rate supercapacitors, J. Phys. Chem. C 120 (2016) 2079–2086.
[39] L. Zhang, F. Zhang, X. Yang, K. Leng, Y. Huang, Y. Chen, High-performance supercapacitor electrode materials prepared from various pollens, Small 9 (2013) 1342–1347.
[40] Y. Lu, S. Zhang, J. Yin, C. Bai, J. Zhang, Y. Li, Y. Yang, Z. Ge, M. Zhang, L. Wei, M. Ma, Y. Ma, Y. Chen, Mesoporous activated carbon materials with ultrahigh mesopore volume and effective specific surface area for high performance supercapacitors, Carbon 124 (2017) 64–71.
[41] Y. Munaiah, B.G.S. Raj, T.P. Kumar, P. Ragupathy, Facile synthesis of hollow sphere amorphous MnO_2: the formation mechanism, morphology and effect of a bivalent cation-containing electrolyte on its supercapacitive behavior, J. Mater. Chem. A 1 (2013) 4300–4306.
[42] P.K. Nayak, N. Munichandraiah, Simultaneous electrodeposition of MnO_2 and Mn $(OH)_2$ for supercapacitor studies, Electrochem. Solid state Lett. 12 (2009) A115–A119.
[43] J. Han, L.L. Zhang, S. Lee, J. Oh, K.-S. Lee, J.R. Potts, J. Ji, X. Zhao, R.S. Ruoff, S. Park, Generation of B-doped graphene nanoplatelets using a solution process and their supercapacitor applications, ACS Nano 7 (2013) 19–26.
[44] X. Tiana, H. Ma, Z. Li, S. Yan, L. Ma, F. Yu, G. Wang, X. Guo, Y. Ma, C. Wong, Flute type micropores activated carbon from cotton stalk for high performance supercapacitors, J. Power Sources 359 (2017) 88–96.
[45] Y. Li, G. Wang, T. Wei, Z. Fan, P. Yan, Nitrogen and sulfur co-doped porous carbon nanosheets derived from willow catkin for supercapacitors, Nanomater. Energy 19 (2016) 165–175.
[46] M.P. Kumar, T. Kesavan, G. Kalita, P. Ragupathy, T.N. Narayanan, D.K. Pattanayak, On the large capacitance of nitrogen doped graphene derived by a facile route, RSC Adv. 4 (2014) 38689–38697.
[47] A.C. Ferrari, J.C. Meyer, V. Scardaci, C. Casiraghi, M. Lazzeri, F. Mauri, S. Piscanec, D. Jiang, K.S. Novoselov, S. Roth, A.K. Geim, Raman spectrum of graphene and graphene layers, Phys. Rev. Lett. 97 (2006) 187401.
[48] L. Miao, D. Zhu, Y. Zhao, M. Liu, H. Duan, W. Xiong, Q. Zhu, L. Li, Y. Lv, L. Gan, Design of carbon materials with ultramicro-, supermicro- and mesopores using solvent- and self-template strategy for supercapacitors, Microporous Mesoporous Mater. 253 (2017) 1–9.
[49] W.-J. Lu, S.-Z. Huang, L. Miao, M.-X. Liu, D.-Z. Zhu, L.-C. Li, H. Duan, Z.-J. Xu, L.-H. Gan, Synthesis of MnO_2/N-doped ultramicroporous carbon nanospheres for high-performance supercapacitor electrodes, Chin. Chem. Lett. 28 (2017) 1324–1329.
[50] P. Ragupathy, H.N. Vasan, N. Munichandraiah, Synthesis and characterization of nano- MnO_2 for electrochemical supercapacitor studies, J. Electrochem. Soc. 155 (2008) A34–A40.
[51] P. Ragupathy, D.H. Park, G. Campet, H.N. Vasan, S.-J. Hwang, J.-H. Choy, N. Munichandraiah, Remarkable capacity retention of nanostructured manganese oxide upon cycling as an electrode material for supercapacitor, J. Phys. Chem. C 113 (2009) 6303–6309.
[52] E.Y.L. Teo, L. Muniandy, E.-P. Ng, F. Adam, A.R. Mohamed, R. Jose, K.F. Chong, High surface area activated carbon from rice husk as a high performance supercapacitor electrode, Electrochim. Acta 192 (2016) 110–119.
[53] J. Hou, C. Cao, X. Ma, F. Idress, B. Xu, X. Hao, W. Lin, From rice bran to high energy density supercapacitors: a new route to control porous structure of 3D carbon, Sci. Rep. 4 (2014) 7260.
[54] H. Feng, H. Hu, H. Dong, Y. Xiao, Y. Cai, B. Lei, Y. Liu, M. Zheng, Hierarchical structured carbon derived from bagasse wastes: a simple and efficient synthesis route and its improved electrochemical properties for high-performance supercapacitors, J. Power Sources 302 (2016) 164–173.
[55] Y. Gong, D. Li, C. Luo, Q. Fu, C. Pan, Highly porous graphitic biomass carbon as advanced electrode materials for supercapacitors, Green Chem. 19 (2017) 4132–4140.
[56] C.-K. Sim, S.R. Majid, N.Z. Mahmood, Electrochemical performance of activated carbon derived from treated food-waste, Int. J. Electrochem. Sci. 10 (2015) 10157–10172.
[57] I.I.G. Inal, S.M. Holmes, A. Banford, Z. Aktas, The performance of supercapacitor electrodes developed from chemically activated carbon produced from waste tea, Appl. Surf. Sci. 357 (2015) 696–703.
[58] D. Wang, G. Fang, T. Xue, J. Ma, G. Geng, A melt route for the synthesis of activated carbon derived from carton box for high performance symmetric supercapacitor applications, J. Power Sources 307 (2016) 401–409.
[59] M. Zhi, F. Yang, F. Meng, M. Li, A. Manivannan, N. Wu, Effects of pore structure on performance of an activated-carbon supercapacitor electrode recycled from scrap waste tires, ACS Sustain. Chem. Eng. 2 (2014) 1592–1598.
[60] L. Zhang, T. You, T. Zhou, X. Zhou, F. Xu, Interconnected hierarchical porous carbon from lignin-derived byproducts of bioethanol production for ultra-high performance supercapacitors, ACS Appl. Mater. Interfaces 8 (2016) 13918–13925.
[61] J. Houa, K. Jiang, M. Tahir, X. Wu, F. Idrees, M. Shen, C. Cao, Tunable porous structure of carbon nanosheets derived from puffed rice for high energy density supercapacitors, J. Power Sources 371 (2017) 148–155.
[62] B.-O. Park, C.D. Lokhande, H.-S. Park, K.-D. Jung, O.-S. Joo, Performance of supercapacitor with electrodeposited ruthenium oxide film electrodes-effect of film thickness, J. Power Sources 134 (2004) 148–152.
[63] M.D. Stoller, R.S. Ruoff, Best practice methods for determining an electrode material's performance for ultracapacitors, Energy Environ. Sci. 3 (2010) 1294–1301.
[64] M.D. Stoller, S. Murali, N. Quarles, Y. Zhu, J.R. Potts, X. Zhu, H.-W. Ha, R.S. Ruoff, Activated graphene as a cathode material for li-ion hybrid supercapacitors, Phys. Chem. Chem. Phys. 14 (2012) 3388–3391.
[65] T. Kesavan, R. Aswathy, I. Arul Raj, T.P. Kumar, P. Ragupathy, Nitrogen-doped graphene as electrode material with enhanced energy density for next-generation supercapacitor application, J. Solid State Sci. Tech 4 (2015) M88–M92.
[66] G.P. Pandey, S.A. Hashmi, Y. Kumar, Performance studies of activated charcoal based electrical double layer capacitors with ionic liquid gel polymer electrolytes, Energy Fuels 24 (2010) 6644–6652.